

1 Visual proteomics using whole-lamella 2D template matching

2

3 This manuscript (permalink) was automatically generated from jojoelfe/deco_lace_template_matching_manuscript@38fd04b
4 on April 14, 2022.

5 **Authors**

- 6 • **Johannes Elferich**  0000-0002-9911-706X ·  jojoelfe RNA Therapeutic Institute, UMass Chan Medical
7 School; HHMI
- 8 • **Nikolaus Grigorieff**  0000-0002-1506-909X ·  nikogrigorieff RNA Therapeutic Institute, UMass Chan
9 Medical School; HHMI

10 **Abstract**

11 Localization of biomolecules inside a cell is an important goal of biological imaging. Fluorescence microscopy
12 can localize biomolecules inside whole cells and tissues, but its ability to count biomolecules and accuracy of the
13 spatial coordinates is limited by the wavelength of visible light. Cryo-electron microscopy (cryo-EM) provides highly
14 accurate position and orientation information of biomolecules but is often confined to small fields of view inside
15 a cell, limiting biological context. In this study we use a new data-acquisition scheme called “Defocus-Corrected
16 Large-Area cryo-EM” (DeCo-LACE) to collect high-resolution cryo-EM data over entire sections (100 – 200 nm thick
17 lamellae) of neutrophil-like mouse cells, representing roughly 1% of the total cellular volume. We use 2D template
18 matching (2DTM) to determine localization and orientation of the large ribosomal subunit in these sections, detect
19 bound small ribosomal subunits and assign ribosomes to polysomes based on their relative orientations to each
20 other. These data provide “maps” of translational activity across sections of mammalian cells. This new high-
21 throughput cryo-EM data collection approach together with 2DTM will advance visual proteomics and complement
22 other single-cell “omics” techniques, such as flow-cytometry and single-cell sequencing.

23 **Introduction**

24 A major goal in understanding cellular processes is the knowledge of the amounts, location, interactions, and
25 conformations of biomolecules inside the cell. This knowledge can be obtained by approaches broadly divided into

26 label- and label-free techniques. In label-dependent techniques a probe is physically attached to a molecule of
27 interest that is able to detected with a high signal-to-noise signal, such as a fluorescent molecule. In label-free
28 techniques the physical properties of molecules themselves are used for detection. An example for this is proteomics
29 using mass-spectrometry [1]. The advantage of label-free techniques is that they can provide information over
30 thousands of molecules, while label-techniques offer highly specific information for a few molecules. Especially
31 spatial information can often only be achieved using label-dependent techniques, such as fluorescence microscopy
32 [2].

33 Cryo-electron microscopy has the potential to directly visualize the arrangement of atoms that compose biomole-
34 cules inside of cells, thereby allowing label-free detection with high spatial accuracy. This has been called “visual
35 proteomics” [3]. Since cryo-EM requires thin samples (<500nm), imaging of biomolecules inside cells is restricted
36 to small organisms, thin regions of cells, or samples that have been suitably thinned. Thinning can be achieved
37 either by mechanical sectioning [4] or by milling using a focused ion beam (FIB) [5]. his complex workflow leads to
38 a low throughput of cryo-EM imaging of cells and is further limited by the fact that at the required magnifications,
39 typical fields of view (FOV) are very small compared to mammalian cells, and the FOV achieved by label-techniques
40 such as fluorescence light microscopy. The predominant cryo-EM technique for the localization of biomolecules of
41 defined size and shape inside cells is cryo-electron tomography [6]. However, the requirement of a tilt series at every
42 imaged location and subsequent image alignment, severely limits the throughput for molecular localization.

43 An alternative approach is to identify molecules by their structural “fingerprint” in single projection using “2D
44 template-matching” (2DTM) [7,8,9]. In this method a 3D model of a biomolecule is used as a template to find 2D
45 projections that match the molecules visible in the electron micrographs. This method requires a projection search
46 on a fine angular grid, and the projections are used to find local cross-correlation peaks with the micrograph. Since
47 the location of a biomolecule in the z-direction causes predictable aberrations to the projection image, this method
48 can be used to calculate complete 3D coordinates and orientations of a biomolecule in a cellular sample [8]

49 Hematopoiesis is the process of generating the various cell types of the blood in the bone marrow. Disregulation
50 of the process results in diseases like leukemia. Understanding how hematopoietic stem and progenitor cells are
51 programmed to diffferentiate to the appropriate cell type would be provide new insight how hematopoiesis can be
52 misregulated. Of special interest is the regulation of translation during hematopoiesis. This is exemplified by the
53 observation that genetic defects in the ribosome machinery often leads to hematopoietic disease[10]. As such direct
54 quantification of ribosome location, number and conformational states could lead to new insight into hematopoietic
55 disease [11].

56 Here we apply 2D-template matching of ribosomes to cryo-FIB milled neutrophil-like murine cells [12]. To in-
57 crease the amount of collected data and to provide unbiased sampling of the whole lamella, we devised a new
58 data-acquisition scheme, Defocus-corrected large area cryo-electron microscopy (DeCo-LACE). We characterize

59 aberration cause by the used large beam-image shifts and highly focused beams and find that they can be ad-
60 equately corrected to enable ribosome detection by 2DTM. The resulting data provide a description of ribosome
61 distribution in the whole lamellae, which represent roughly 2% of the cellular volume. We find highly heterogeneous
62 density of ribosome within the cell and can identify discrete clusters of presumably translationally active ribosomes,
63 by testing for the presence of the small ribosomal subunit. The high accuracy of location and orientation of each
64 detected ribosome also allows us to cluster ribosome molecules into potential polysomes. Analysis of the throughput
65 in this method suggests that for the foreseeable future computation will be the bottleneck for visual proteomics.

66 Materials and Methods

67 Grid preparation

68 ER-HoxA9 cells were maintained in RPMI medium supplemented with 10% FBS, penicillin/streptomycin, SCF, and
69 estrogen [12] at 37C and 5% CO₂. 120h prior to grid preparation, cells were washed twice in PBS and cultured in
70 the same medium except without estrogen. Differentiation was verified by staining with Hoechst-dye and inspection
71 of nuclear morphology. Cells were then counted and diluted to 1 · 10⁶ cells/ml. Grids (either 200 mesh copper grids,
72 with a silicone-oxide and 2um holes with a 2um spacing or 200 mesh gold grids with a thin gold film and 2 um holes
73 in 2um spacing) were glow-discharged from both sides using a 15 mA for 45s . 3.5 ul of cell suspension was added
74 to grids on the thin-film side and grids were automatically blotted from the back side using a GP2 cryoplunger
75 (Leica) for 8 s and rapidly plunged into liquid ethane at -185°C.

76 FIB-milling

77 Grids were loaded into a Acquilos 2 FIB/SEM microscope with a stage cooled to -190°C. Grids were sputter-coated
78 with platinum for 15s at 45 mA and then coated with a layer of platinum-precursor by opening the GIS-valve for 45s.
79 An overview of the grid was created by montaging SEM images and isolated cells at the center of gridsquares were
80 selected for FB-milling. Lamella were generated automatically using the AutoTEM software, with the following
81 parameters:

- 82 • Milling angle: 20°
- 83 • Rough milling: 3.2 μm thickness, 0.5nA current
- 84 • Medium milling: 1.8 μm thickness, 0.3nA current, 1.0° overtilt
- 85 • Fine milling: 1.0 μm thickness, 0.1nA current, 0.5° overtilt
- 86 • Finer milling: 700 nm thickness, 0.1nA current, 0.2° overtilt
- 87 • Polish 1: 450nm thickness, 50 pA current
- 88 • Polish 2: 200nm thickness, 30 pA current

89 This resulted in 6-8 um wide lamella with 150-250nm thickness as determined by FIB-imaging of the lamella edge.

90 **Data collection**

91 Grids were loaded into a Krios Titan TEM (Thermore Fisher) operated at 300 keV and equipped with a BioQuantum
92 energy filter (Gatan) and K3 camera (Gatan). The microscope was aligned using a cross-grating grid on the
93 stage. Prior to each session we carefully performed the Image/Beam calibration in nanoprobe. Then we set the
94 magnification to a pixel size of 1.76Å and condensed the beam to ~ 900nm diameter, resulting in the beam being
95 completely visible on the camera. To establish fringe-free conditions, the “Fine eucentric” procedure of serialEM
96 was used to move a square of the cross-grating grid to the eucentric position of the microscope. The effective defocus
97 was then set to 2 um, using the “autofocus” routine of serialEM. The objective focus of the microscope was changed
98 until no fringes were visible. The stage was then moved in Z until images had a apparent defocus of 2 um. The
99 difference in stage Z-position between the eucentric and fringe-free conditions was then used to move other areas
100 into fringe-free condition.

101 Low magnification montages were used to find lamella and lamella that were sufficiently thin and free of contamina-
102 tion were selected for automated data collection. Vverview images of each lamella were taken at 2250x magnification
103 (39Å pixel-sixe). The corners of the lamella in the overview image were manually annotated in SerialEM and trans-
104 lated into Beam-Imageshift values using SerialEM calibration. A hexagonal pattern of Beam-Imageshift positions
105 was calculated that covered the area between the four corners in a serpentine way, with a $\sqrt{3} * 400$ nm horizontal
106 spacing and 800 nm vertical spacing. Exposures were then taken at each position with a 30 e/Å² total dose. After
107 each exposure that defocus was estimated using the ctffind function of SerialEM and the focus for the next exposure
108 was corrected by the difference between the estimated focus and the desired defocus of 800 nm. Furthermore, after
109 each exposure the deviation of the beam from the center of the camera was measured and corrected using the
110 “CenterBeamFromImage” command of SerialEM.

111 After datacollection a 20s exposure at 2250x magnification of the lamella at 200um defocus was taken for visualiza-
112 tion purposes. A python script implementing this procedure is available at [Link to repo].

113 **Data pre-processing**

114 To avoid influence of the beam-edge on motion-correction only a quarter of the movie in the center of the camera
115 was considered for calculation of the estimated motion. After movie frames were aligned and summed a mask for
116 the illuminated area was calculated by lowpass filtering the image at 100Å, thresholding the image at 10% of the
117 maximal value and then lowpass filtering the mask at 100Å. This mask was then used to replace un-illuminated
118 area with gaussian noise, with the same mean and standard deviation as the illuminated area. A custom version
119 of the unblur program implementing this procedure is available at (TODO). The contrast-transfer function (CTF)
120 was estimated using ctffind, searching between 0.02 and 2 um defocus.

121 **2DTM**

122 The search template was generated from the cryo-EM structure of the mouse large ribosomal subunit (PDB 6SWA)
123 using the simulate program in cisTEM [cite]. The atomic coordinates corresponding to Epb1 were deleted from
124 the model and the simulate program of the cisTEM suite was used to calculate an density map from the atomic
125 coordinates. The match_template program was used to search for this template in the preprocessed images, using
126 1.5° angular step in out-of-plane angles and 1.0° in-plane. 11 defocus planes in 20nm steps centered around the
127 defocus estimates by ctffind were searched. Matches were defined as peaks above a threshold of 7.75, which was
128 chosen based on a one false positive per tile criterium [cite].

129 **DeCo-LACE data processing**

130 An overview of the data analysis pipeline is shown in Fig. 6. Initial coordinates of each Tile i , $\mathbf{c}_{init,i}$ were derived
131 from the Beam-Image-Shift of the tile BIS_i and the ISToCamera matrix \mathbf{IC} :

$$\mathbf{c}_{init,i} = \mathbf{IC} \cdot BIS_i$$

132 To refine the montage a list of overlapping tile pairs $|\mathbf{c}_i - \mathbf{c}_j| < 900\text{nm}$ were compiled and the offsets $\mathbf{o}_{i,j} = \mathbf{c}_i - \mathbf{c}_j$
133 were refined by using a masked cross-correlation of the overlap region as implemented in the scikit-image package
134 [cite]. Refined coordinates were then derived by minimizing the least-deviation of the new offsets and tile positions:

$$\min \sum_{pairs} (\mathbf{o}_{refined,i,j} - (\mathbf{c}_i - \mathbf{c}_j))^2$$

135 using the scipy package [cite]. This refinement was then repeated once more.

136 The x,y coordinates of 2DTM match n in the tile i , $\mathbf{m}_{n,i}^T$, was transformed into the montage frame by adding the
137 coordinate of the tile.

$$\mathbf{m}_n^M = \mathbf{m}_{n,i}^T + \mathbf{c}_i$$

138 The z coordinate of each match was calculated as the sum of the defocus offset for each match, the estimated
139 defocus of the tile, and the nominal defocus of the microscope when the tile was acquired. The python scripts used
140 are available under [repolink].

¹⁴¹ **Results**

¹⁴² **2DTM detects large ribosomal subunits in cryo-FIB lamella of mammalian cells**

¹⁴³ To test whether we could detect individual ribosomes in mammalian cells we prepared cryo-lamella of mouse
¹⁴⁴ neutrophil-like cells. Low-magnification images of these lamellas clearly shows cellular features consistent with a
¹⁴⁵ neutrophil-like phenotype, mainly a segmented nucleus and a plethora of membrane-organelles, corresponding to
¹⁴⁶ the granules and secretory vesicles of neutrophils (Fig. 1A). We then proceeded to acquire micrographs on this
¹⁴⁷ lamella with a defocus of 0.5-1.0 um, 30 e/Å²/s exposure and 1.5 Å pixelsize. We manually selected multiple
¹⁴⁸ locations in the lamella and acquired micrographs using standard low-dose techniques where focusing is performed
¹⁴⁹ on a sacrificial area. The resulting micrographs showed no signs of crystalline ice and smooth bilayered membranes
¹⁵⁰ (Fig. 1C,D), indicating successful vitrification.

¹⁵¹ We used an atomic model of the 60S mouse ribosomal subunit (6SWA) for 2DTM. In a subset of images the
¹⁵² distribution of cross-correlation scores significantly exceeded the distribution expected from non-significant matching.
¹⁵³ In the resulting scaled maximum-intensity maps, clear peaks with SNR thresholds up to 10 were apparent (Fig.
¹⁵⁴ S1A). By using the criterion described by for thresholding potential matches we found that in images of cytosolic
¹⁵⁵ compartments we found evidence of 10-500 ribosomes in the imaged areas (Fig. 1B-E). Notably, we found no
¹⁵⁶ matches in images areas corresponding to the nucleus (Fig. 1B) or mitochondria (Fig. 1D). In the cytosolic areas we
¹⁵⁷ found a drastically different number of matches, In some areas we found only ~ 50 matches per image area (Fig.
¹⁵⁸ 1E), while in another area we found more than 500 matches (Fig. 1C). This ten-fold difference in local ribosome
¹⁵⁹ concentration , but we realized that current data acquisition protocols are limited in that only a small area of the
¹⁶⁰ lamella is actually imaged and, due to the manual selection of acquisition positions based on the overview image,
¹⁶¹ might be biased towards cellular region that appear appealing to the experimentalist. We therefore set out to collect
¹⁶² cryo-EM data for 2DTM from mammalian lamella in a high-throughput unbiased fashion.

¹⁶³ **DECO-LACE for 2D imaging of whole lamella**

¹⁶⁴ In order to obtain high-resolution data for complete lamella we used a new approach for data collection. This
¹⁶⁵ approach uses three key strategies: (1) ensures that every electron that exposes the sample is collected on the
¹⁶⁶ camera (2) uses beam-image shift to precisely and quickly raster the surface of the lamella and (3) uses a focusing
¹⁶⁷ strategy that does not rely on a sacrificial area (Fig. 2A).

¹⁶⁸ To ensure that every electron exposing the sample was captured by the detector, we focused the electron beam so
¹⁶⁹ that the entire beam was placed on the detector. During canonical low-dose imaging the microscope is configured
¹⁷⁰ so that the focal plan is identical to the eucentric plane of the specimen stage. This leaves the C2 aperture out of
¹⁷¹ focus, resulting in ripples at the edge of the beam (Fig. 2D). While these ripples are low-resolution features that
¹⁷² might not interfere with 2D template matching, which is designed to be robust to low-resolution noise, we also

173 tested collecting data under a condition where the C2 aperture is in focus (Fig. 2E).

174 We then centered a lamella under the electron beam and used beam-image shift of the microscope to systematically
175 raster the whole surface of the lamella in a hexagonal pattern(Fig. 2A,C). Instead of focusing in a sacrificial area,
176 we determined the defocus after every exposure by fitting the Thon rings. The focus was then adjusted based on the
177 difference between desired and measured defocus (Fig. 2B). Since we used a serpentine pattern for data collection
178 every exposure is close to the previous exposure making drastic changes in the defocus unlikely. Furthermore we
179 started our acquisition pattern on the platinum deposition edge, so the initial exposure where the defocus was not
180 yet adjusted did not contain any biologically relevant information.

181 We used this strategy to collect data on 8 lamella, 4 using the eucentric focus condition, from hereon referred to as
182 Lamella_{EUC}, and 4 using the fringe-free condition, from hereon referred to as Lamella_{FFF}(Fig. S2). We were able to
183 highly consistently collect data with a defocus of 800nm (Fig. 2F), both in the eucentric focus and fringe-free focus
184 condition. To ensure that data was collected consistently, we mapped defocus values as a function of the applied
185 Beam-image shift (Fig. S3A). This demonstrated that the defocus was consistent over the lamella, with outliers
186 only at isolated images and in images containing contamination. We also plotted the measure objective astigmatism
187 of the lamella and found that it varies with the applied Beam-image shift, become more astigmatic mostly due to
188 beam-image shift in the X direction(Fig. S3B). While approaches exist to correct this during the data-collection
189 [cite], we opted to not use these approaches in our initial experiments. We reasoned that because 2DTM depends
190 on high-resolution information, this would be an excellent test of how much these aberration affect imaging.

191 We assembled the tile micrographs into a montage using the Beam-Image-shift value and the SerialEM calibration
192 followed by cross-correlation based refinement (see Methods). In the resulting montages the same cellular features
193 than in the overview images are apparent (Fig. S3G-J), however due to the high magnification and low defocus
194 many more details, such as the membrane bilayer seperation can be observed. For montages collected using the
195 eucentric there are clearly visible fringes at the edges between the tiles, which are absent in the fringe-free focus
196 montage. However, it is unclear whether these fringes impede molecular detection or due to their low-resolution
197 nature are only an aesthetic issue. We also note that the tiling pattern is visible in the montages, which we believe
198 is due to the non-linear behaviour of the K3 camera (see Dicussion).

199 While inspecting the montages we noticed that the membrane vesicles and granules are highly variable in size and
200 electron density of their content. We found furthermore that a substantial number of granules with a high electron
201 density seemed to contain a membrane-enclosed inclusion with electron-density similar to the surrounding cytosol
202 (Fig. [TODO]). [Describe measurements]

203 **2DTM of DeCo-LACE data reveals ribosome distribution in cellular cross-sections**

204 In initial attempts of using 2DTM on micrographs acquired with the DeCo-LACE protocol, we did not observe any
205 SNR peaks above threshold using the large subunit of the mouse ribosome (Fig. S4A). We reasoned that the edges
206 of the beam might interfere with motion-correction of the movie as they would remain stationary or move differently
207 than the sample. Indeed when we cropped movie to exclude the beam edges we found that the estimated motion
208 was larger than estimated on the uncropped movie (Fig. S4B). Furthermore, in the motion-corrected average we
209 could identify SNR peaks above detection threshold (Fig. S4B), indicating that 2DTM is very sensitive to accurate
210 motion correction and that the beam edge did interfere with motion-correction. In order to avoid having to crop
211 the movies we implemented a function in unblur to consider only the cropped area for estimation of shifts, but
212 average the complete movie (Fig. S4B). Using this approach we motion-corrected all tiles in the 8 lamella and
213 found consistently total motion below 1Å per frame (Fig. S5 A). In some lamella we found increased motion in the
214 center of the lamella, which indicates that mechanical stability of FIB-milled lamella might not be homogeneous
215 over the lamella surface. In some micrographs we also observed that the beam edges gave rise to artifacts in the
216 cross-correlation mip and numerous false-positive matches at the edge of the illuminated area (Fig. TODO). A
217 similar phenomenon was observed on isolated “hot” pixels in the unilluminated area. To overcome this issue we
218 implemented a function in unblur to replace unilluminated areas in the micrograph with gaussian noise, with mean
219 and standard deviation matched to the illuminated portion of the micrograph (Fig. TODO). Together, these special
220 pre-processing steps enabled us to perform 2DTM on all tiles of the 8 lamellae.

221 We then used the refined tile positions to calculate the positions of the matched LSUs in the lamellae (Fig. 4
222 A, Fig. 5 A). Overlaying these positions of the lamella montages reveal ribosome distribution throughout the FIB-
223 milled slice of individual cells. Organelles like the nucleus and mitochondria only showed sporadic matches with
224 low SNRs, consistent with the estimated false-positive rate on one per tile. During the assembly we calculated the
225 Z positions from the individual estimated defocus levels and the focus plane of the microscope during acquisition of
226 each tile. When viewed from the side the ribosome position therefore show the slope of the lamella in the microscope
227 frame (Fig. 4 B, Fig. 5 B). Furthermore, the side-views indicated that lamellae were thinner at the leading edge.
228 Indeed, when we plotted the electron intensities in individual tiles as a function of Beam-Image shift we observed
229 substantially higher intensities at the leading edge, which in energy-filtered TEM indicates a thinner sample [cite].
230 Even though we prepared the lamellae with the “overtile” approach [cite], this means that ribosome densities across
231 the lamellae can be skewed by the changes in thickness and better sample preparation methods are needed to
232 generate more even samples.

233 Close inspection of the ribosome positions in the lamellae revealed multi interesting features. Ribosomes could be
234 seen associating with the membrane, in patterns reminiscent of the rough endoplasmic reticulum (Fig. 4 C, Fig.
235 5 C) or the outer nuclear membrane (Fig. 4 D). We also observed ribosomes forming ring-like structures (Fig. 4

236 E), potentially indicating circularized mRNAs [cite]. While ribosomes were for the most part excluded from the
237 numerous granules observed in the cytoplasm, in some circumstances we observed clusters of ribosomes in the lower
238 electron density inclusion in the class of double-membraned granules described earlier (Fig. 4 F, Fig. 5 D,E). It is,
239 in principle, possible that these matches are situated above or below the imaged granule, since the granules position
240 in Z cannot be determined using a 2D projection. However, in the case of Fig. 5 E, the matched ribosomes span
241 the whole lamella in the Z direction, while a position above or below the granule would result in ribosome situated
242 exclusively at the top or bottom of the lamella. This conclusive evidence of ribosomes in the inclusion is consistent
243 with the earlier hypothesis that the inclusion is of cytoplasmic origin.

244 Between the 8 lamellae we found different number of matches (Fig. 3 A). Lamella_{EUC} 1 resulted in the most matches,
245 but also has the largest surface area and contained cytoplasm of two cells. Lamella_{FFF} 4 had the fewest matches,
246 but this particular slice was dominated by a circular nucleus slice, with only small pockets of cytoplasm (Fig. S2).
247 In an attempt to normalize for these differences in lamella surface area we compared the number of matches per
248 tile in tiles which contained more than one match, which should exclude tiles with non-cytosolic content (Fig. 3 B).
249 While this measure had less variability, there were still differences. Lamella_{EUC} 4 had not only the fewest matches,
250 but also the lowest density, which could be due to the thickness of the lamella or due to a slice through low-ribosome
251 content region. Lamella_{FFF} 3 had substantially higher number of ribosomes per tile. Since all of these lamella were
252 milled into identical cells under identical conditions, this underscores the necessity to collect data on large numbers
253 of lamella in order to overcome inherent variability. When comparing the distribution of scores between the lamella
254 we found them to be fairly comparable with a median of Lamella_{EUC} 1 had slightly lower scores compared
255 to others, potentially due to the large size and connected mechanical instability during imaging. Overall we did
256 not observe a difference in number or SNR of matches between eucentric or fringe-free focus illumination that was
257 bigger than inter-lamella variability.

258 Since the SNR values of 2DTM are highly sensitive to image quality we reasoned we could use them to verify that
259 DeCo-LACE does not introduce systematic errors. We first wondered whether the unusually condensed beam would
260 be prone to non-parallel illumination or whether at the outside of the beam unknown aberration would distort the
261 image. We reasoned that this would lead to lower SNR values at the inside edge of the illuminated area. When
262 we plotted SNR values in all 8 lamellae as a function of their location in tiles we found high SNR value up to the
263 edge of the illuminated area for both eucentric and fringe-free focus illumination, again demonstrating that both
264 illumination schemes are suitable for DeCo-LACE.

265 We also wondered whether high Beam-Image shift values would lead aberration due to the astigmatism or beam
266 tilt [cite]. [TODO plot scores vs BIS, euc vs fff]

267 **Computation is the bottleneck of visual proteomics**

268 As described above the variability of lamella, both in terms of technique such as area, thickness and mechanical
269 stability, and of biology, such as selection of cell and location of the slice in relation to the complete cell, could be
270 overcome by collecting orders of magnitude more data. This will be essential to allow robust statistical comparisons
271 of macromolecule number and location between different experimental conditions.

272 **Discussion**

- 273 • Elizabeth Wright and Grant Jensen Montage tomography papers
- 274 • Waffle method for higher throughput, automation of fib-milling
- 275 • Throughput and bottlenecks
- 276 • lamella mechanical properties, radiation damage, other ways to to thin?
- 277 • eucentric vs fringe free illumination
- 278 • Visual proteomics
- 279 • Granules containing ribosomes?
- 280 • Threshold implications (no matches on most images)
- 281 • K3 not linear

282 **Figures**

283 **References**

- 284 1. **Label-free, normalized quantification of complex mass spectrometry data for proteomic analysis** Noelle M Griffin, Jingyi Yu, Fred Long, Phil Oh, Sabrina Shore, Yan Li, Jim A Koziol, Jan E Schnitzer
Nature Biotechnology (2010-01) <https://doi.org/fshgnc> DOI: 10.1038/nbt.1592 · PMID: 20010810 · PMCID: PMC2805705
- 285 2. **Fluorescence microscopy** Jeff W Lichtman, José-Angel Conchello
Nature Methods (2005-11-18) <https://doi.org/bbpg4n> DOI: 10.1038/nmeth817 · PMID: 16299476

287

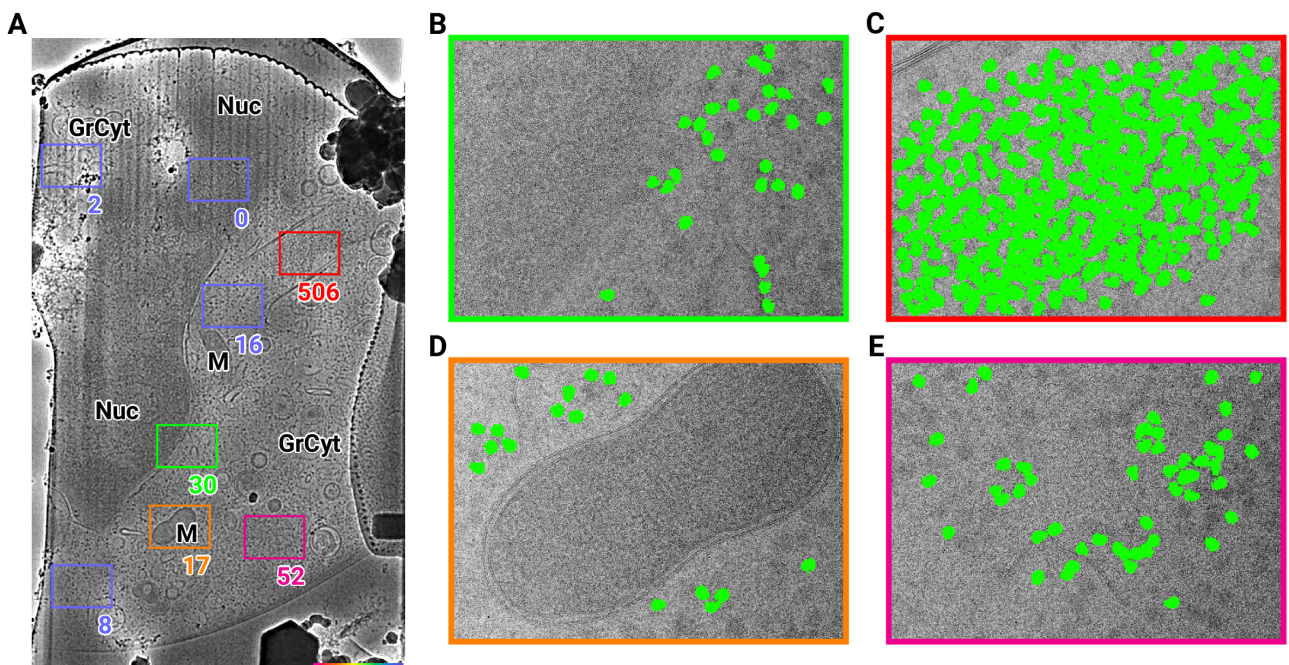


Figure 1: 2D template matching of the large subunit of the ribosome in fib-milled neutrophil-like cells (A) Overview image of the lamella. Major cellular regions are labeled, as Nucleus (Nuc), Mitochondria (M), and granular cytoplasm (GrCyt). FOVs where high-magnification images for template matching were acquired are indicated as boxes with the number of matches indicated on the bottom right. FOVs displayed in Panels B-E are color-coded. (B-E) FOVs with projection of ribosome LSU matches shown in green. (B) Perinuclear region, the only matches are in the cytoplasmic half. (C) Cytoplasmic region with high density of ribosomes (D) Mitochondrion, as expected there are only matches in the cytoplasmic region (E) Cytoplasm, with low density of ribosomes.

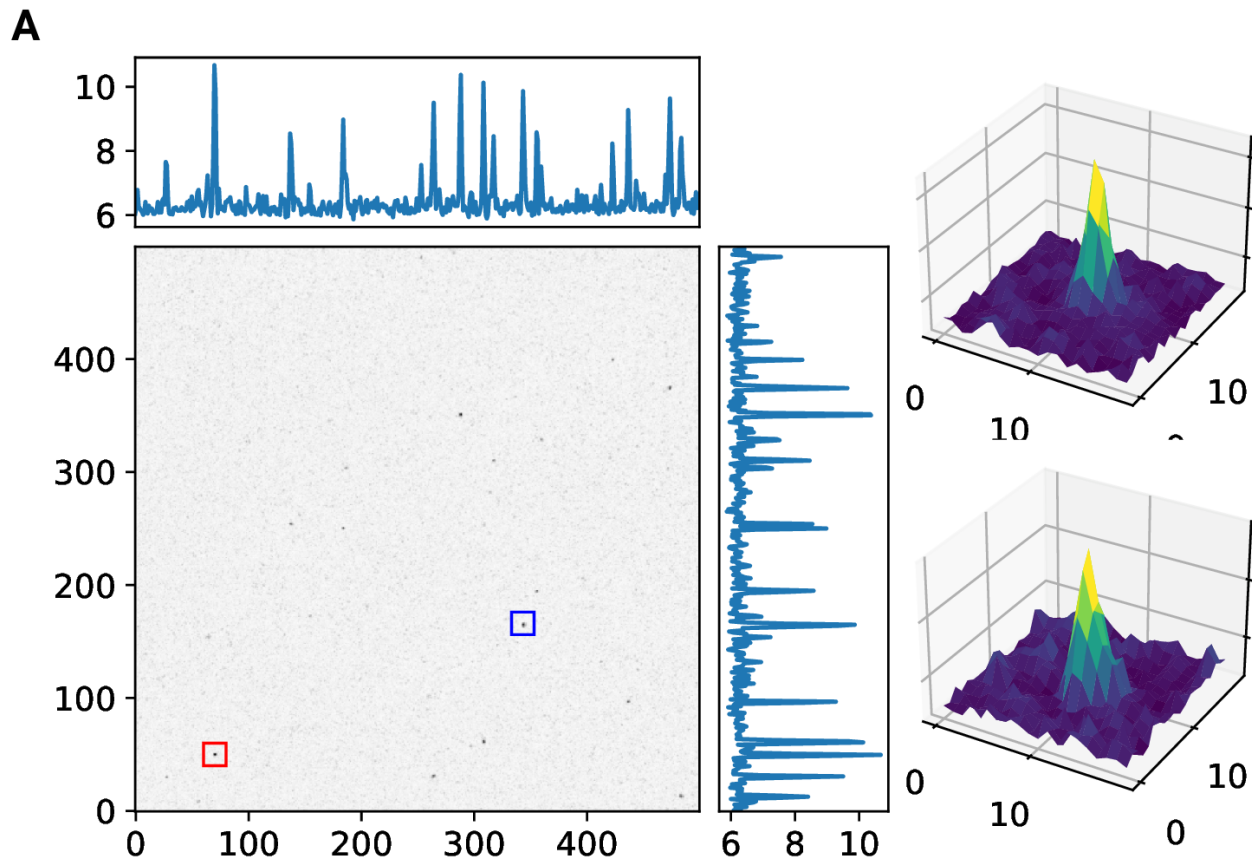


Figure S1: 2D template matching of the large subunit of the ribosome in fib-milled neutrophil-like cells (A) Maximum intensity projection cross-correlation map of micrograph shown in Figure 1 (B+C) 3D plot of MIP regions indicated by color boxes in Panel A

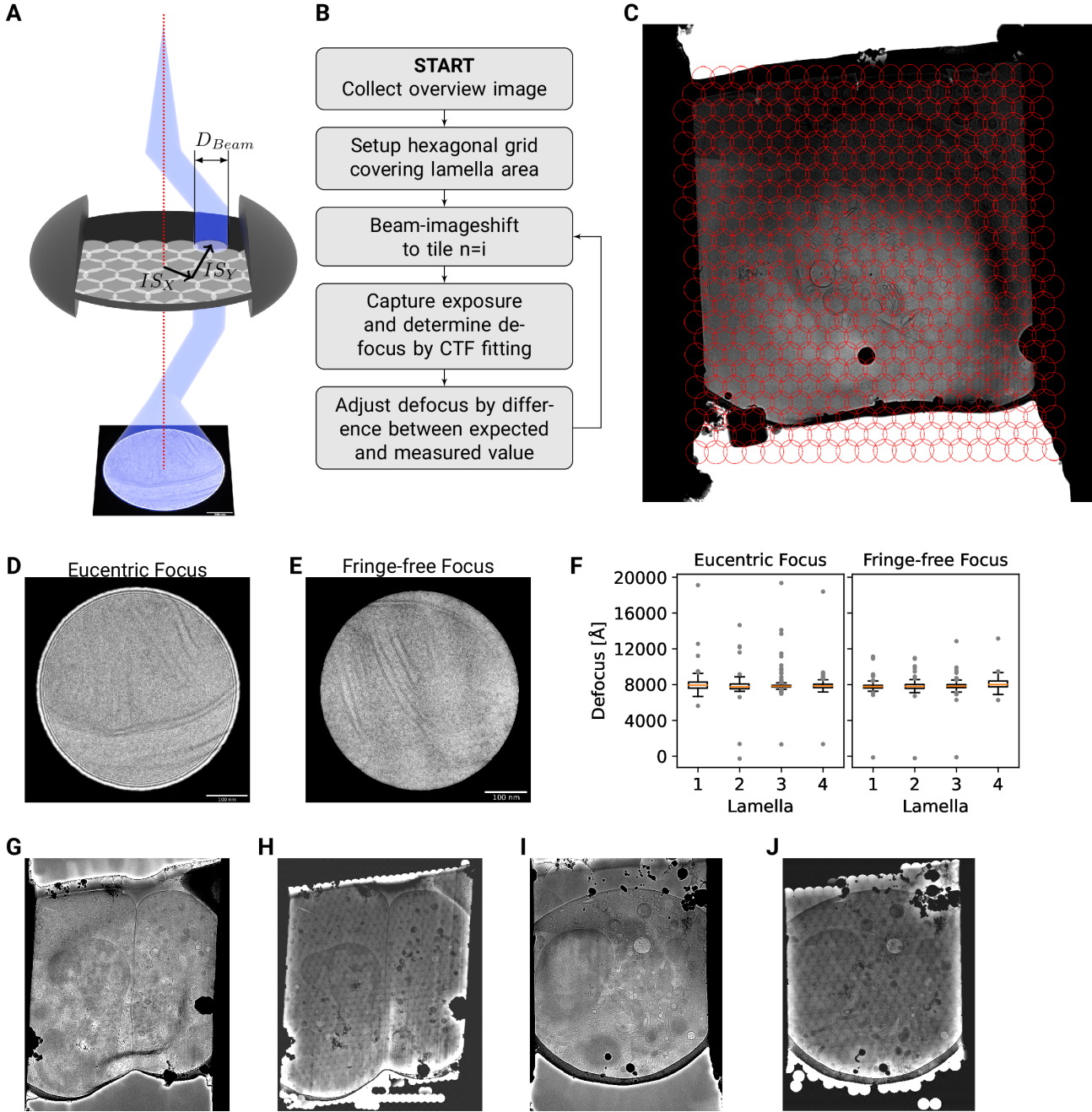


Figure 2: DeCo-LACE approach (A) Graphic demonstrating the data-collection strategy for DeCo-LACE. The electron beam is condensed to a diameter D_{Beam} that allows captured of the whole illuminated area on the camera. Beam-image shift along X and Y (BIS_X, BIS_Y) is used to raster the whole lamella (B) Diagram of the collection algorithm (C) Example overview image of a lamella with the designated acquisition positions and the used beam diameter indicated with red circles (D+E) Representative micrographs taken with a condensed beam at eucentric focus (D) or fringe-free focus (E) (F) Boxplot of defocus measured by ctffind of micrographs taken by the DeCo-Lace approach on 4 lamella images at eucentric focus and 4 lamella imaged with fringe-free focus. (F+G) Lamella overview images of lamella imaged at eucentric focus (F) Overview image taken at low magnification (40 Å pixel size) (G) Overview created by montaging high magnification images taken with the DeCo-Lace approach (1.5 Å pixelsize) (H+I) Lamella overview images of lamella imaged at fringe-free focus (H) Overview image taken at low magnification (40 Å pixel size) (I) Overview created by montaging high magnification images taken with the DeCo-Lace approach (1.5 Å pixelsize)

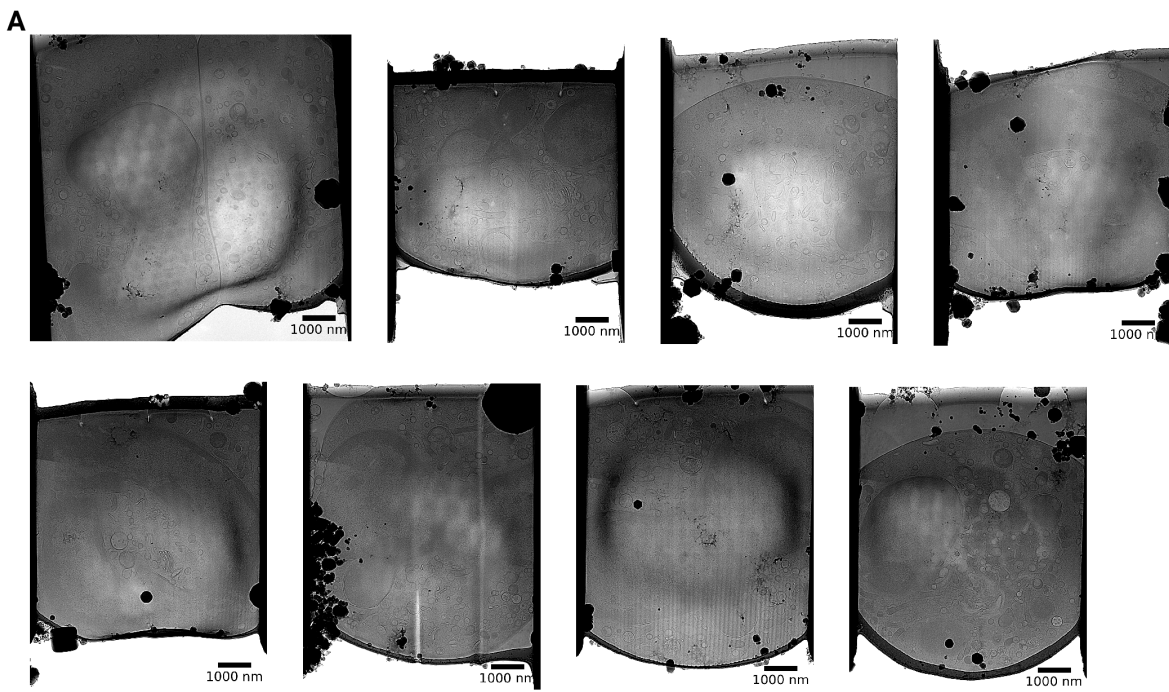


Figure S2: Overview images of lamellae imaged using the DeCo-LACE approach taken at low-magnification

288 3. **A visual approach to proteomics** Stephan Nickell, Christine Kofler, Andrew P Leis, Wolfgang Baumeister

Nature Reviews Molecular Cell Biology (2006-02-15) <https://doi.org/d6d5mq> DOI: 10.1038/nrm1861 ·
PMID: 16482091

289

290 4. **Electron microscopy of frozen hydrated sections of vitreous ice and vitrified biological samples**

AW McDowall, J-J Chang, R Freeman, J Lepault, CA Walter, J Dubochet
Journal of Microscopy (1983-07) <https://doi.org/bdnzmv> DOI: 10.1111/j.1365-2818.1983.tb04225.x ·
PMID: 6350598

291

292 5. **Opening windows into the cell: focused-ion-beam milling for cryo-electron tomography**

Elizabeth Villa, Miroslava Schaffer, Jürgen M Plitzko, Wolfgang Baumeister
Current Opinion in Structural Biology (2013-10) <https://doi.org/f537jp> DOI: 10.1016/j.sbi.2013.08.006 ·
PMID: 24090931

293

294 6. **Electron tomography of cells** Lu Gan, Grant J Jensen

Quarterly Reviews of Biophysics (2011-11-15) <https://doi.org/czj9hr> DOI: 10.1017/s0033583511000102 ·
PMID: 22082691

295

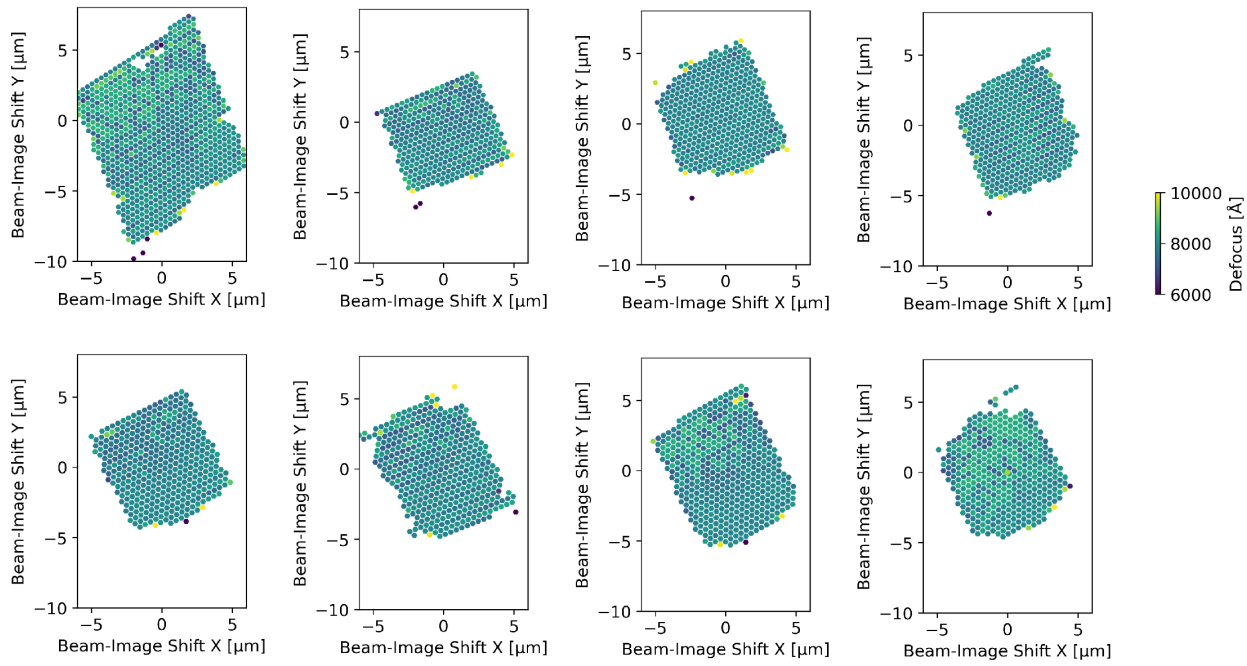
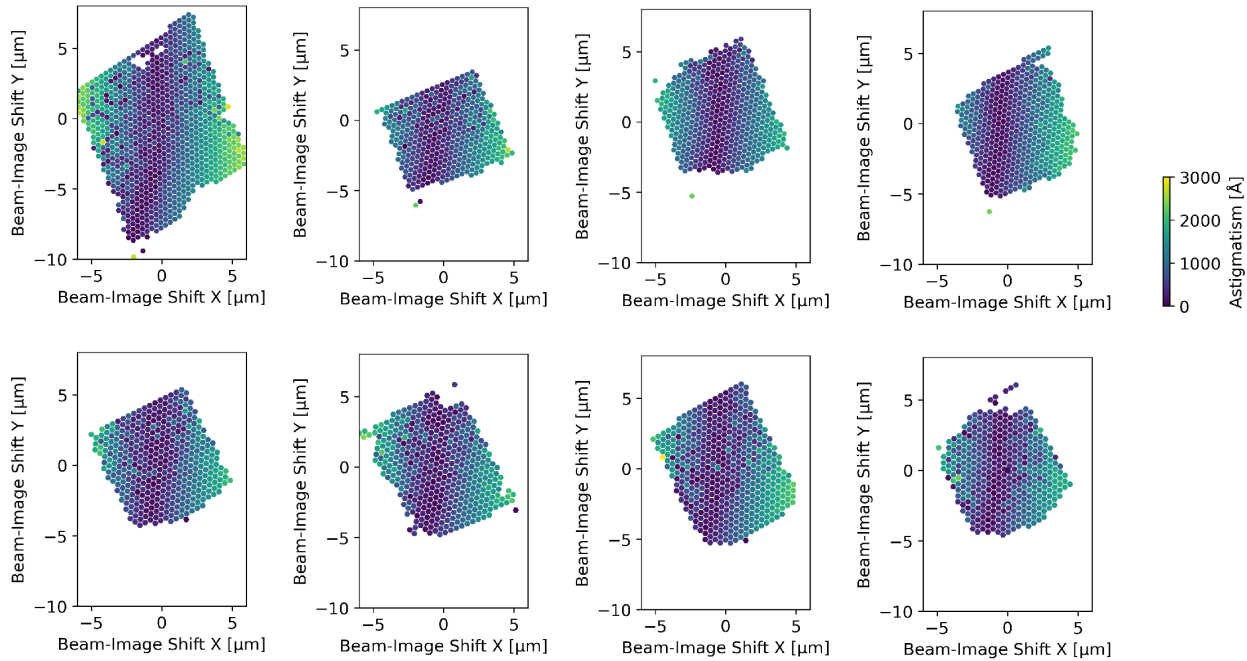
A**B**

Figure S3: Defocus estimation of individual tiles of DeCo-Lace montages (A) Defocus values of individual micrographs taken using the DeCo-Lace approach plotted as a function of the Beam-Image-Shift values. (B) Defocus astigmatism of individual micrographs taken using the DeCo-Lace approach plotted as a function of the Beam-Image-Shift values.

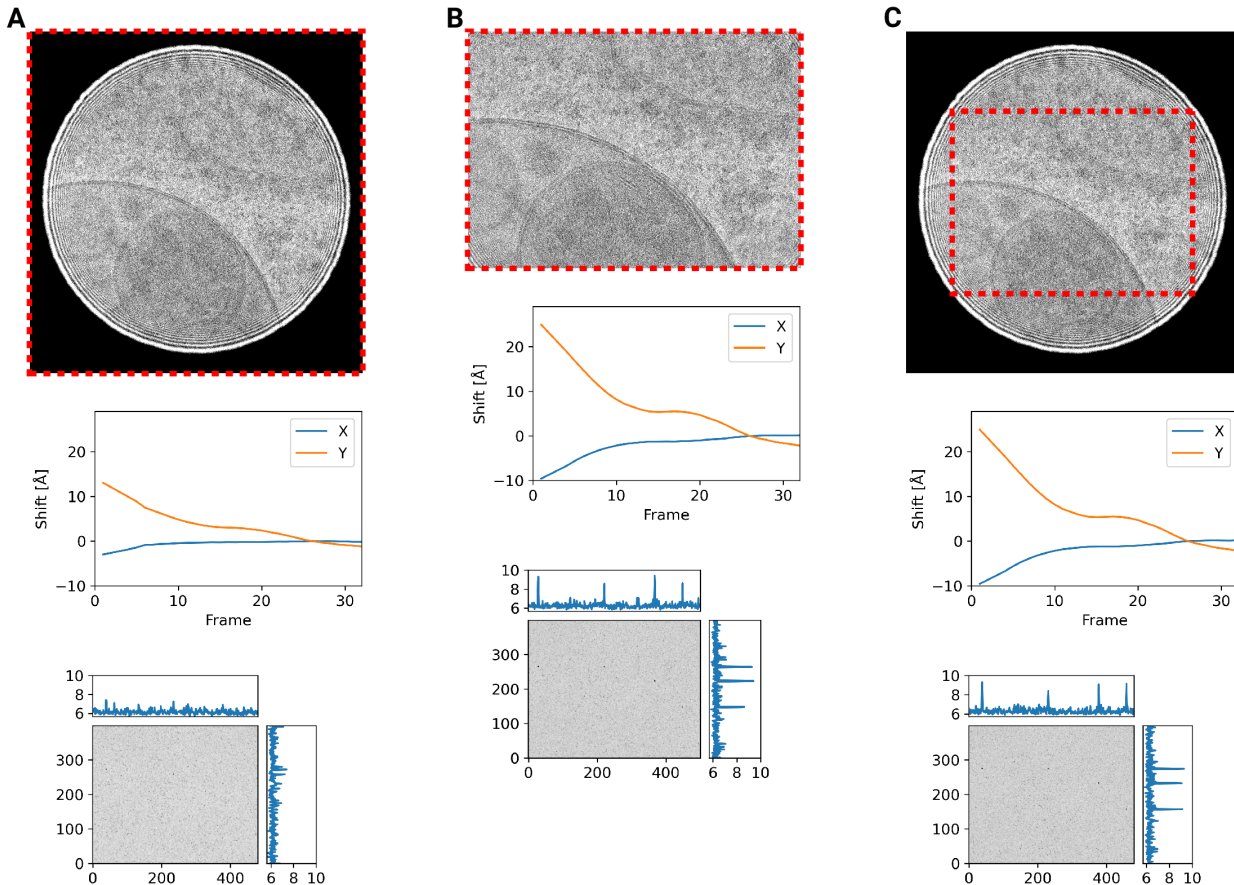


Figure S4: Motion correction of movies with condensed beams. At the top of each panel is an average of the movie that was motion-corrected with a red dashed box indicating the region that was used to estimate shifts. Below is a graph indicating the estimated shifts of the individual frames of the movie. Below this is the MIP of 2DTM using the large subunit of the mouse ribosome. (A) Motion correction of the whole movie (B) Motion correction of a cropped region of the movie that eliminates the beam edges (C) Motion correction of the whole movie, using only the cropped region to estimate the shifts

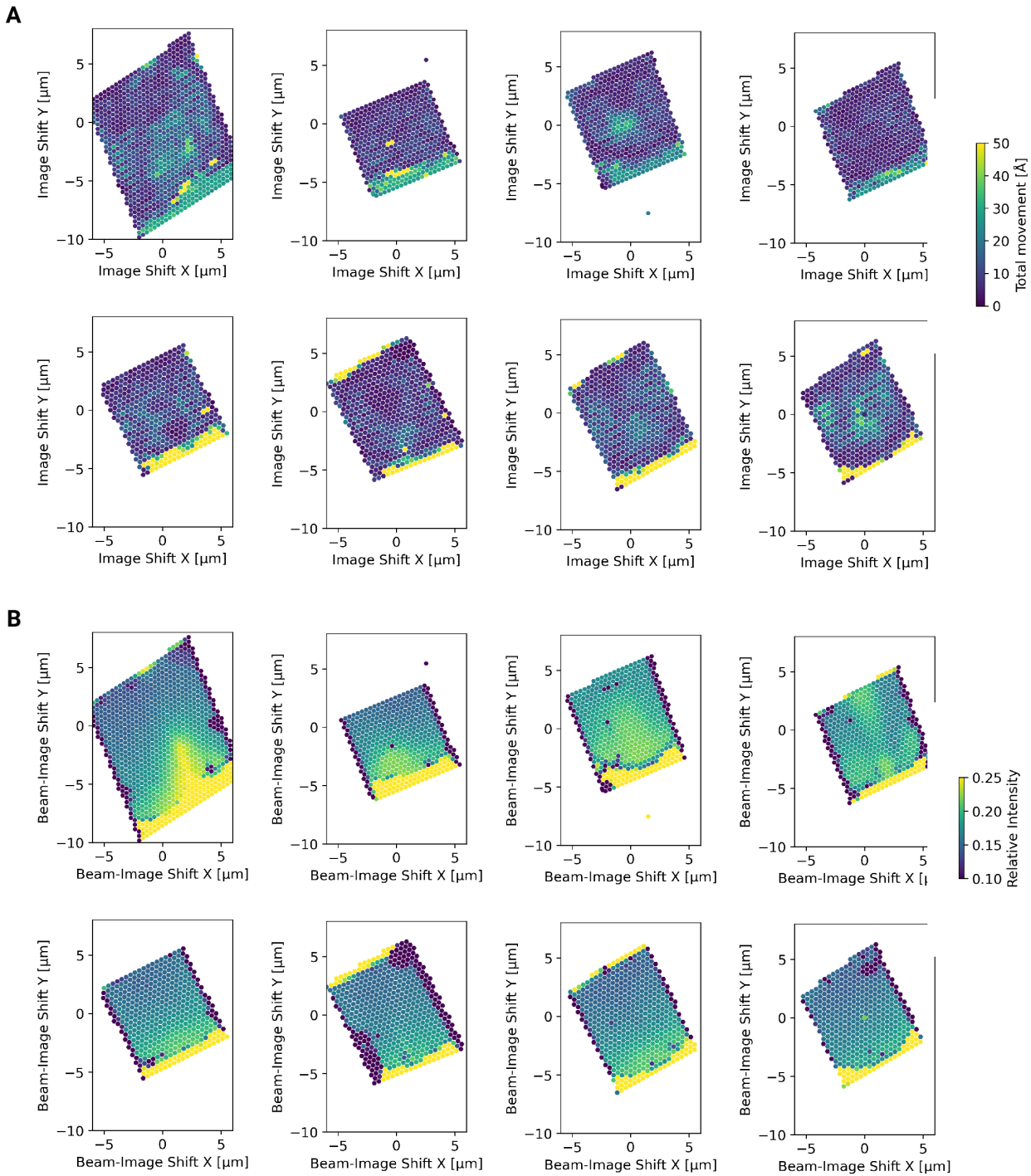


Figure S5: Motion correction of individual tiles imaged using the DeCo-LACE approach (A) Total estimated motion of individual micrographs taken using the DeCo-Lace approach plotted as a function of the Beam-Image-Shift values. (B) Electron intensity of individual micrographs taken using the DeCo-Lace approach plotted as a function of the Beam-Image-Shift values.

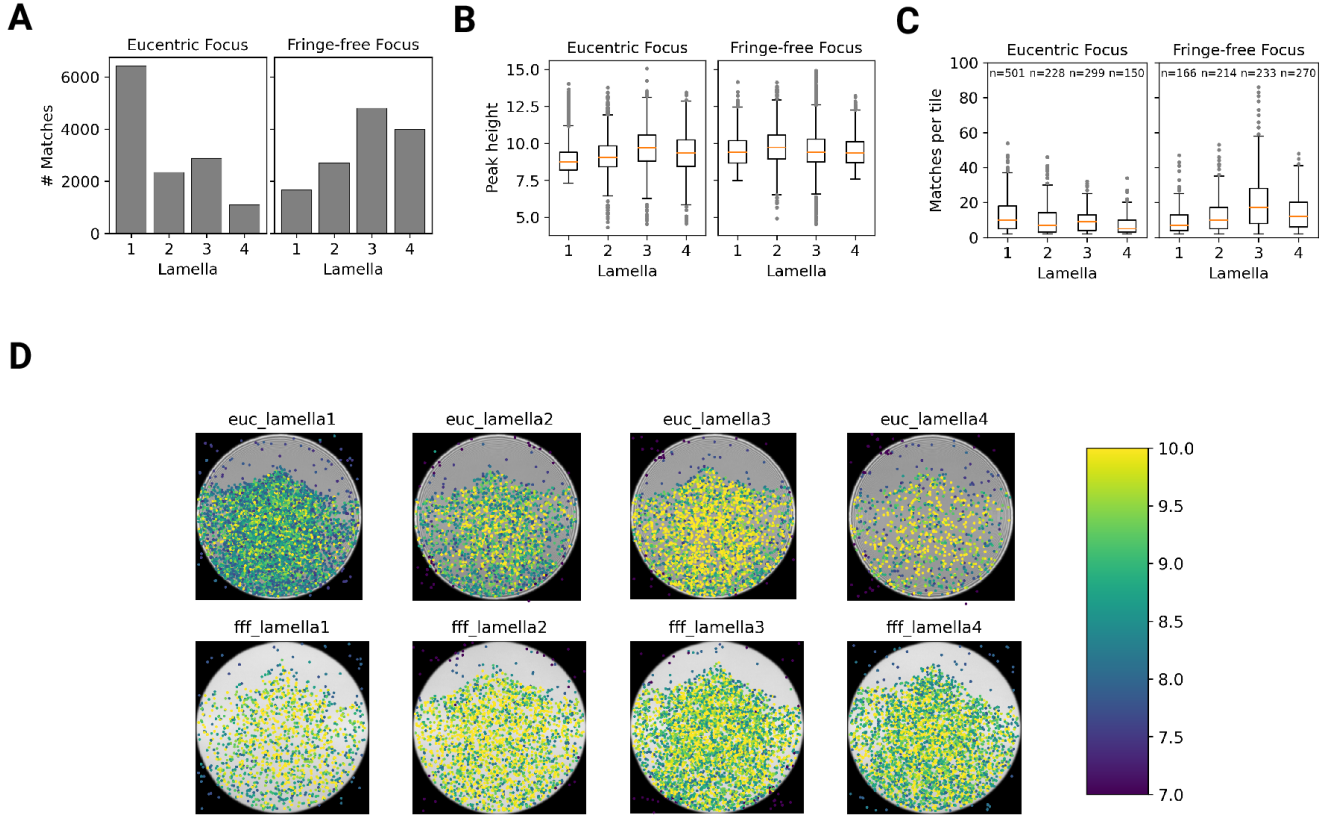


Figure 3: Statistics of 2DTM on lamella imaged using DeCo-LACE (A) Number of matches of each lamella (B) Distribution of matches per tile in each lamella. Only tiles with two or more matches were included (C) Distribution of SNRs in each lamella (D) For each lamella an average of all tiles is shown. Overlaid is a scatterplot of all matches in these tiles according to their in-tile coordinates. Scatterplot is color according to the SNR. There are no matches in the top circle-circle intersection due to radiation damage from previous exposures.

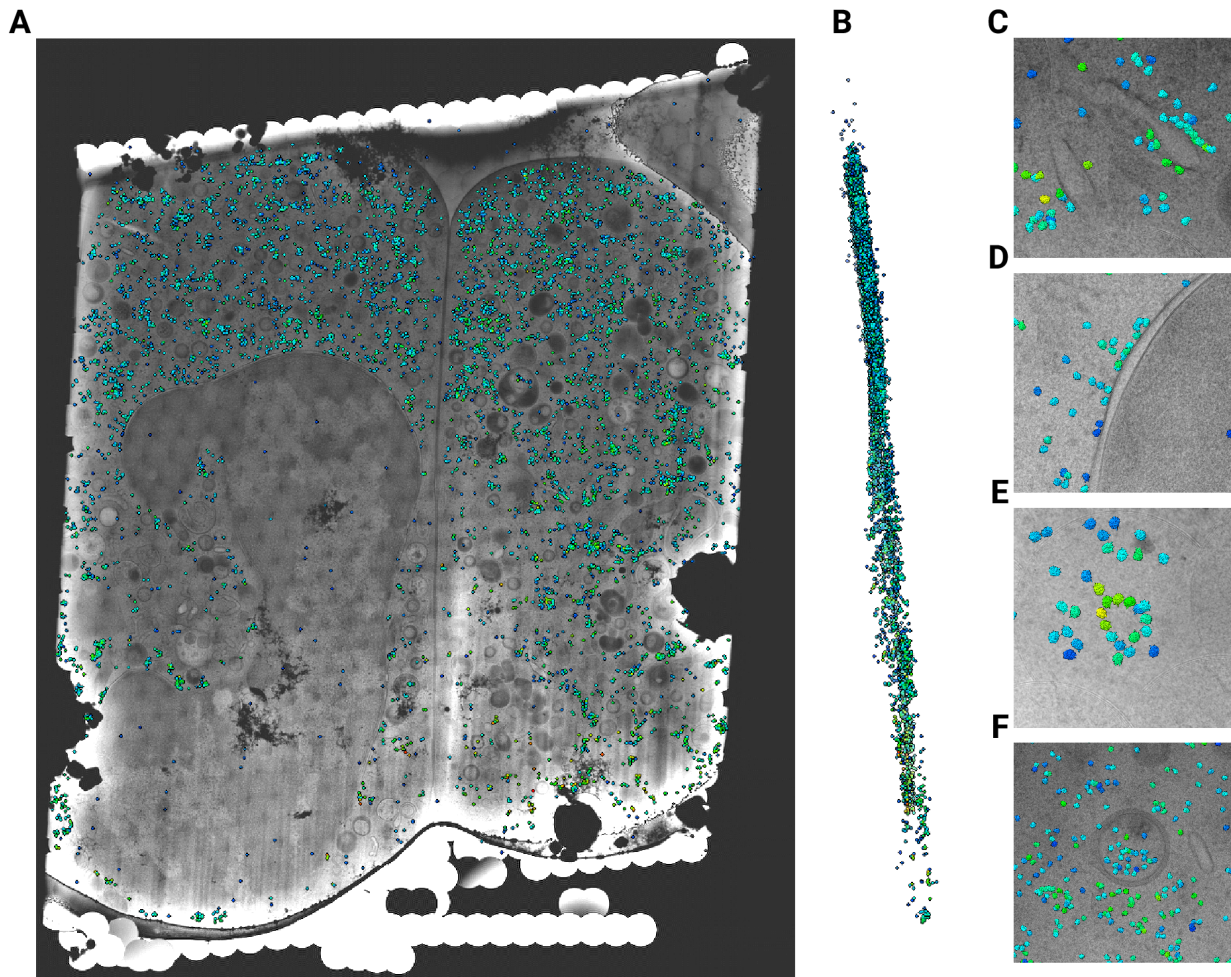


Figure 4: Template matching in lamella imaged using the DeCo-Lace approach at eucentric focus (A) Montage of Lamella_{EUC} 1 overlaid with matches according to their montage coordinates (B) Side view of matches in the lamella, such that the direction of the electron beam is horizontal. (C-F) Magnified area of panel A showing rough ER with associated ribosomes(C), outer nuclear membrane with associated ribosomes (D), ribosomes arranged in a circular fashion(E), ribosomes enclosed in a less electron dense inclusion in a granule(F).

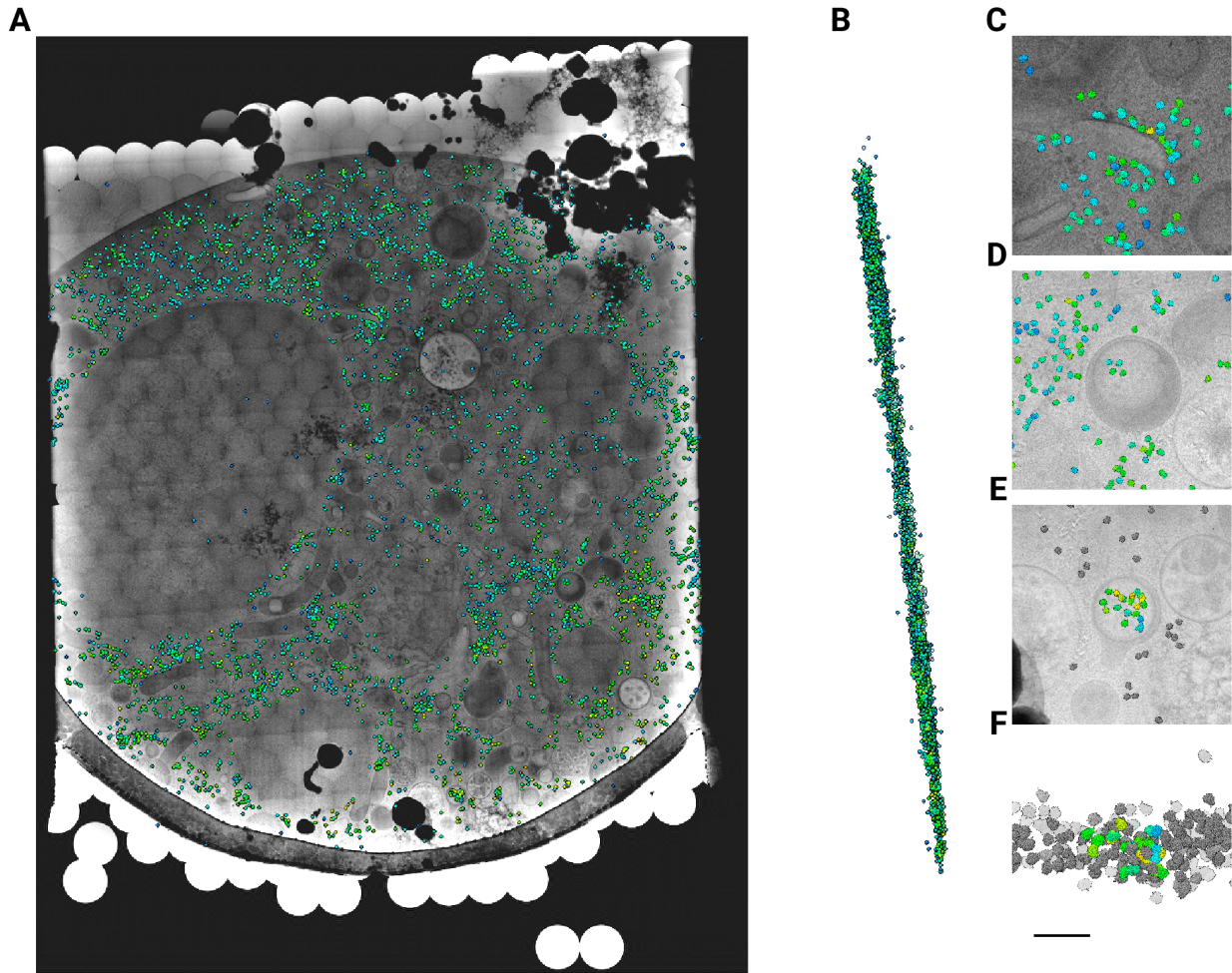


Figure 5: Template matching in lamella imaged using the DeCo-Lace approach at fringe-free focus (A) Montage of Lamella_{FFF} 4 overlaid with matches according to their montage coordinates (B) Side view of matches in the lamella, such that the direction of the electron beam is horizontal. (C-E) Magnified area of panel A showing rough ER with associated ribosomes(C) and ribosomes enclosed in a less electron dense inclusion in a granule(D,E). (F) Side view of panel E with ribosomes situated inside the granule colored according to SNR and other ribosomes colored in grey.

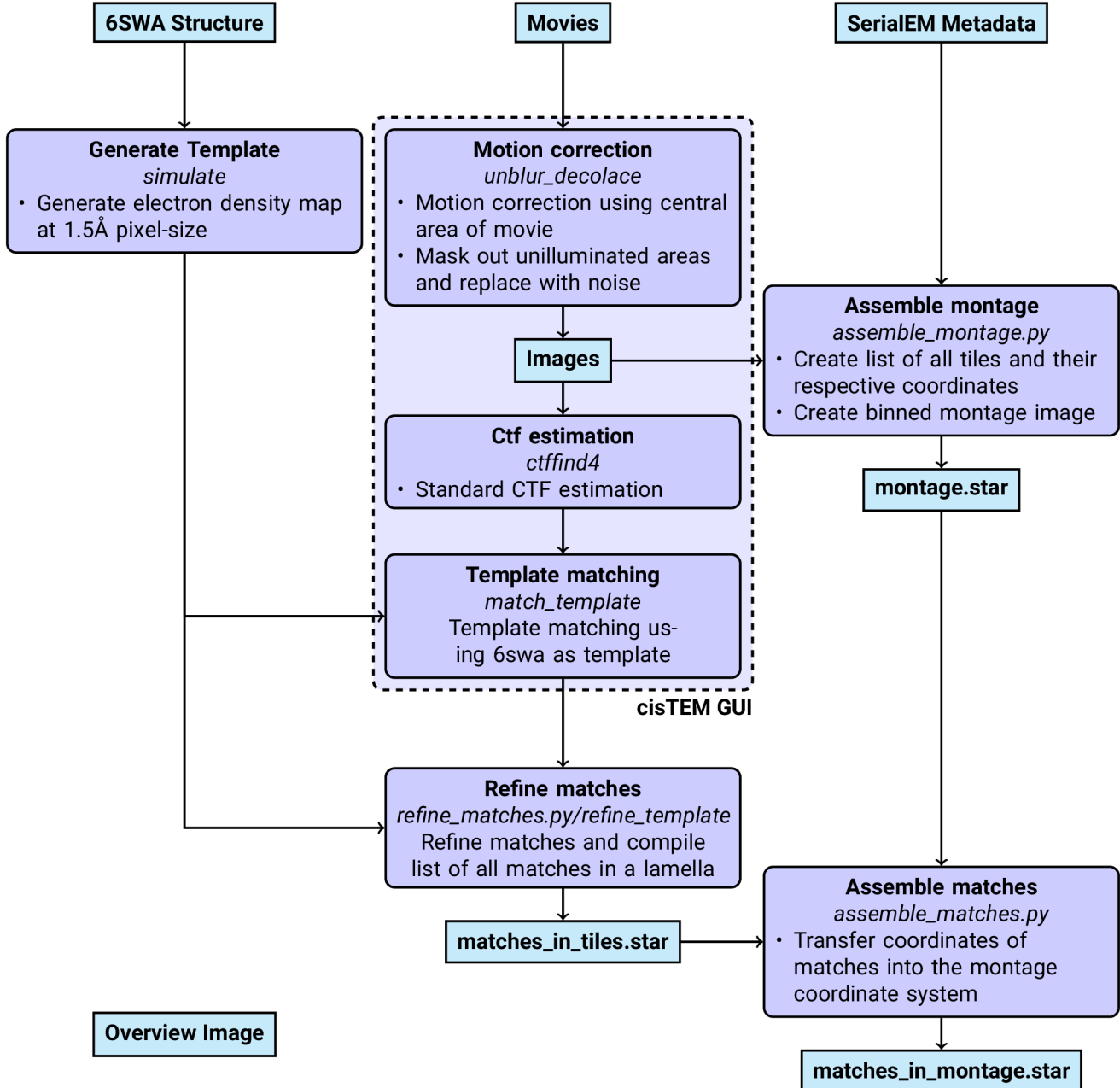


Figure 6: Workflow of DeCo-Lace processing

- 296 7. **Single-protein detection in crowded molecular environments in cryo-EM images** JPeter Rickgauer, Nikolaus Grigorieff, Winfried Denk
eLife (2017-05-03) <https://doi.org/gnq4q4> DOI: 10.7554/elife.25648 · PMID: 28467302 · PMCID: PMC5453696
- 297
- 298 8. **Label-free single-instance protein detection in vitrified cells** JPeter Rickgauer, Heejun Choi, Jennifer Lippincott-Schwartz, Winfried Denk
Cold Spring Harbor Laboratory (2020-04-24) <https://doi.org/gpbjfd> DOI: 10.1101/2020.04.22.053868
- 299
- 300 9. **Locating macromolecular assemblies in cells by 2D template matching with cisTEM** Bronwyn A Lucas, Benjamin A Himes, Liang Xue, Timothy Grant, Julia Mahamid, Nikolaus Grigorieff
eLife (2021-06-11) <https://doi.org/gkkc49> DOI: 10.7554/elife.68946 · PMID: 34114559 · PMCID: PMC8219381
- 301
- 302 10. **Hallmarks of ribosomopathies** Kim R Kampen, Sergey O Sulima, Stijn Vereecke, Kim De Keersmaecker
Nucleic Acids Research (2019-07-27) <https://doi.org/gpbjfm> DOI: 10.1093/nar/gkz637 · PMID: 31350888 · PMCID: PMC7026650
- 303
- 304 11. **Diagnostic and prognostic implications of ribosomal protein transcript expression patterns in human cancers** James M Dolezal, Arie P Dash, Edward V Prochownik
BMC Cancer (2018-03-12) <https://doi.org/gc87j9> DOI: 10.1186/s12885-018-4178-z · PMID: 29530001 · PMCID: PMC5848553
- 305
- 306 12. **Inhibition of Dihydroorotate Dehydrogenase Overcomes Differentiation Blockade in Acute Myeloid Leukemia** David B Sykes, Youmna S Kfouri, François E Mercier, Mathias J Wawer, Jason M Law, Mark K Haynes, Timothy A Lewis, Amir Schajnovitz, Esha Jain, Dongjun Lee, ... David T Scadden
Cell (2016-09) <https://doi.org/f3r5jr> DOI: 10.1016/j.cell.2016.08.057 · PMID: 27641501 · PMCID: PMC7360335